

# Femtosecond Imbalanced Time-Stretch Spectroscopy

Haiyun Xia<sup>1,2,3,†,\*</sup>, Zhen Zhang<sup>1,†</sup>, Saifen Yu<sup>1</sup>, Lijie Zhao<sup>1</sup>, Tianwen Wei<sup>1</sup>, Manyi Li<sup>1</sup>, Mingjia Shangguan<sup>1</sup>, Chong Wang<sup>1</sup>, Jiawei Qiu<sup>1</sup>, Xiankang Dou<sup>1,2,3,4</sup>

<sup>1</sup>CAS Key Laboratory of Geospace Environment, University of Science and Technology of China, Hefei 230026, China

<sup>2</sup>Hefei National Laboratory for Physical Sciences at the Microscale, University of Science and Technology of China, Hefei, 230026, China

<sup>3</sup>CAS Center for Excellence in Comparative Planetology, University of Science and Technology of China, Hefei, 230026, China

<sup>4</sup>School of Electronic Information, Wuhan University, Wuhan, 430072, China

†These authors contributed equally to this work.

\*e-mail: hsia@ustc.edu.cn

**Dual-comb spectroscopy is a promising method for precise optical spectrum analysis with fast data acquisition speed. However, its implementation and applications are often hindered by the complexity of optical comb systems. Here, as a compact and robust system, femtosecond imbalanced time-stretch spectroscopy (FITSS) with simple optical layout is proposed and demonstrated. The time-stretch interferometry from one femtosecond laser builds a mapping from the optical frequency domain to the radio frequency regime. In experiment, the absorption line of a hydrogen cyanide cell is encoded in the probing arm of a Mach-Zehnder interferometer (MZI). The down-converted radio frequency comb is transformed from a periodically chirped waveform, which is the interferogram of the MZI with different dispersion values on two arms. By turning the optical filter, the spectrum over a wide range is analyzed.**

Ultrafast spectroscopy has been a crucial tool for understanding the substance composition, molecular evolution and kinetics in not only fundamental sciences of physics, chemistry and biomedicine, but also applied domains of gas tracing and leakage warning. As the widely used spectroscopy in the past decades, Fourier transform spectroscopy (FTS) provides broad-band spectrum and well-resolved data in non-intrusive diagnostics of molecular structures in various media. Recently, researchers are focusing on new methods with characteristics of fast acquisition time, high sensitivity, high resolution and broad spectral bandwidth. With the revolution of optical frequency (OF) metrology brought by stabilized optical frequency combs, dual-comb spectroscopy DCS<sup>1-6</sup> emerges as a powerful scheme covering the above characteristics and equipping with no moving components. DCS with two coherent optical frequency combs holds much promise for laboratorial precision spectroscopy<sup>7,8</sup> and regional comprehensive sensing<sup>9,10</sup>. However, in the process of advancing to practical applications, it is hindered by complexity of two optical combs with stabilized pulse repetition frequency ( $f_{rep}$ ) and carrier-envelope offset frequency ( $f_{ceo}$ ). Despite daunting technical challenges, great efforts of research communities are devoted to enhance the performance of dual-comb laser for a compact and stable DCS, incorporating different techniques, such as microresonators<sup>11-14</sup>, electro-optic modulation<sup>4</sup> and one cavity comb<sup>15,16</sup>.

Another ultrafast technique called time-stretch<sup>17</sup> plays an important role not only in ultrafast single-shot

spectroscopy<sup>18-20</sup>, imaging<sup>21-23</sup>, ranging<sup>24,25</sup> and other measurements of non-repetitive and statistically rare signals<sup>26</sup>, but also in ultra-wideband<sup>27</sup> and chirped<sup>28,29</sup> microwave pulses generation for high speed communications and radars. Time-stretch builds a time-to-frequency mapping by introducing group delay dispersion (GVD) using various dispersion devices, such as optical fiber, chirped fiber Bragg grating and angular dispersion device. However, time-stretch often suffers from low signal-to-noise ratio (SNR) due to high insertion loss of the adopted dispersion device. So amplifiers are employed to ensure real-time detection in most cases<sup>17,18</sup>. On the other way, the SNR can be improved by incorporating heterodyne detection, where the weak signal is mixed with a strong local oscillator, resulting in a radio frequency (RF) beat signal. For example, in the ultrafast ranging system<sup>24,25</sup>, a non-chirped RF waveform is generated for ultrafast ranging purpose. However, due to its narrow-band RF spectrum, the spectrum information encoded in the envelope is hard to be acquired. Interestingly, by introducing imbalanced dispersion in the Mach-Zehnder interferometer (MZI), a chirped interferogram with ultra-wideband (UWB) RF is generated, where the information carried on the optical spectrum is down-converted to the UWB-RF spectrum.

As shown in Fig. 1, in the time-stretch heterodyne detection, the probing and reference pulses are split from one femtosecond laser, so that the two pulses have intrinsic coherence. If there is no imbalanced dispersion in the MZI (Fig. 1a), a non-chirped RF waveform is generated and the RF spectrum has a narrow bandwidth. While in Fig. 1b, an imbalanced dispersion is added to the reference pulse. Within one period, the time spacing between neighboring frequency teeth are different in two arms. Here dual-comb source is obtained from the single femtosecond laser without phase-locked loop, which is much simpler than DCS using two phase-locked combs. The heterodyne detection produces a chirped RF pulse, which carries the spectrum information. Thus gas absorption feature encoded in optical spectrum can be retrieved in the envelope of the UWB-RF combs. Here, femtosecond imbalanced time-stretch spectroscopy (FITSS) is implemented by using one femtosecond laser, inheriting features from both time-stretch and DCS, such as down-conversion ability from the OF domain to the RF domain, high detection sensitivity, and ultrafast data-acquisition.

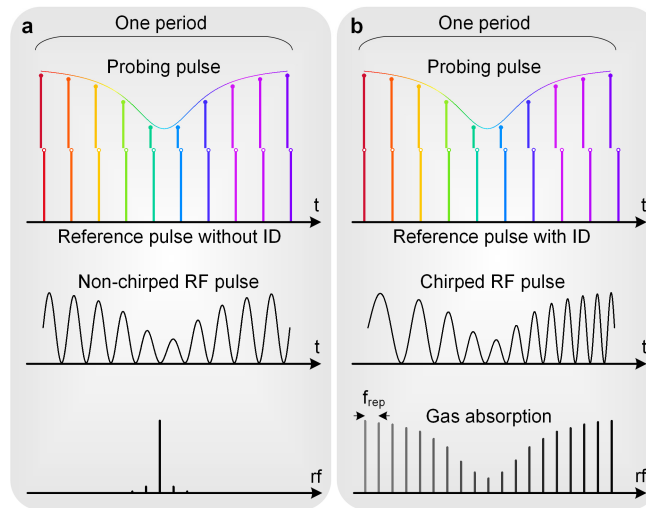


**Fig. 1 | Comparison between time-stretch heterodyne detection with imbalanced dispersion (ID) and without imbalanced dispersion. a**, Without imbalanced dispersion. **t**: time. **b**, With imbalanced dispersion. The figures from top to bottom are frequency comb teeth in the stretched probing pulse, frequency comb teeth in the stretched reference pulse, interferograms after heterodyne detection and RF combs, respectively.

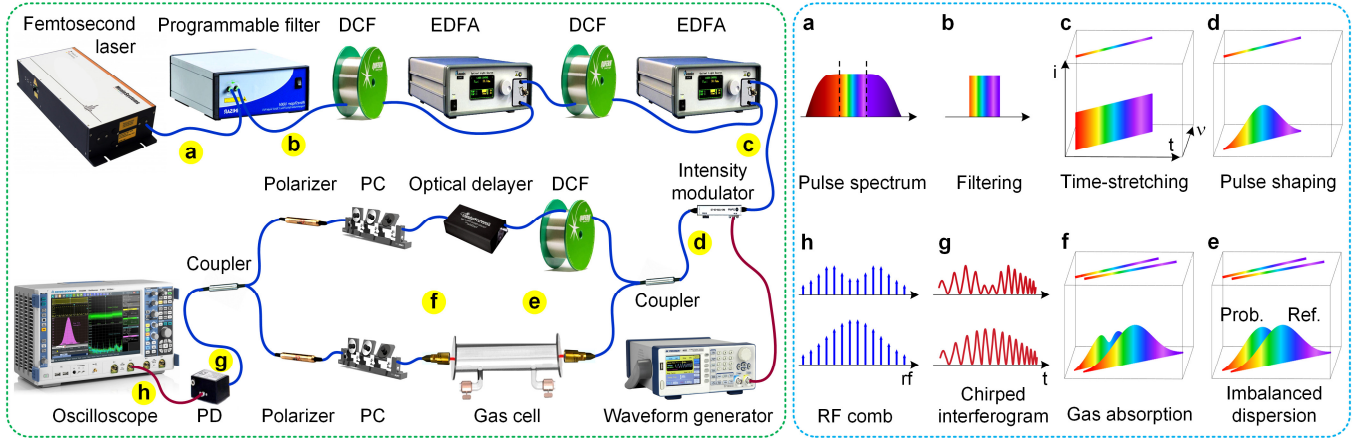


**Fig. 2 | The optical layout of FITSS (in the left dash line box) and the spectra and pulses (in the right dash line box) at different stages (labeled as (a) - (h)).** a, The femtosecond laser spectrum is tailored to b, the range of interest by a programmable filter. c, The stretched laser pulse shown in the time-frequency space. t: time. v: optical frequency. i: intensity. d, Gaussian shaped pulse. e, Probing pulse and reference pulse in the MZI without H<sup>13</sup>CN gas. f, Pulses after gas absorption in the probing arm. g, Electric interferogram on the detector. h, FFT results in the oscilloscope. DCF: dispersion compensation fiber. EDFA: erbium-doped fiber amplifier. PC: polarization controller. PD: photodiode.

The principle of FITSS is to perform Fourier transform on a periodically chirped time domain waveform, which is the interferogram of a MZI with different dispersion values on two arms. The optical layout of FITSS is shown in the left dash line box of Fig. 2. The spectra and pulses at different stages (labeled as (a) - (h)) is show in the right dash line box. A femtosecond laser with stabilized pulse with repetition rate of 100 MHz serves as the laser source (a). The femtosecond pulse is tailored in the spectrum domain to cover the spectrum range of one absorption line by a programmable filter with a bandwidth of 0.9 nm (b). Then the pulse is stretched (c) in the time-stretch module consisting of cascaded DCFs with sufficient dispersion value and EDFAs to compensate the power loss. The optical pulse after dispersion is illustrated in the time-frequency space as shown as Fig. 2c. The total dispersion value of time-stretch module is 14.5 ns/nm. The pulse duration is stretched from tens of femtoseconds to about ten nanoseconds. In order to suppress the sideband effects due to rectangular window function introduced by the programmable filter, an intensity modulator driven by a waveform generator is employed to tailor the pulse in the time domain with Gaussian shape (d), as shown in Fig. 2d. Then, the pulse is split into two pulses in the MZI (Fig. 2e and 2f). The reference pulse transmits through an additional DCF with dispersion of 3.3 ns/nm, resulting in different time-to-frequency mapping function relative to the probing pulse, as shown in Fig. 2e (see details in Methods). The probing pulse transmits through a H<sup>13</sup>CN gas cell (48 cm, 100 Torr) with the spectrum shown in Fig. 2f. The time delay between the two pulses is adjusted by using an optical delayer. The MZI incorporates temperature control and vibration isolation for stabilizing the phase difference between two arms. After going through polarization controllers and in-line polarizers, the pulses are combined by a coupler for heterodyne detection (see details in Methods). A chirped interferogram (Fig. 2g) with period of 10 ns is detected in a photodiode and recorded in an oscilloscope with sampling rate of 80 Giga samples per second. The bottom interferogram in Fig. 2g is formed without H<sup>13</sup>CN gas cell. Finally, by performing fast Fourier transformation (FFT) on the periodically chirped interferogram, the absorption feature is shown in the RF comb (Fig. 2h).

The former DCS establishes a direct link between OF domain and RF domain by employing two coherent combs with

slightly different repetition rates. Although DCS offers marked improvements in spectral resolution, sensitivity and data-acquisition speed, the demanding mutual-coherence requirements are mostly achieved with complex stabilization or synchronization including several stabilization loops and highly nonlinear processes. In contrast, here, the spectrum down-conversion is realized by using one femtosecond laser and imbalanced dispersion in the time-stretch interferometry, making the system simple thus robust.

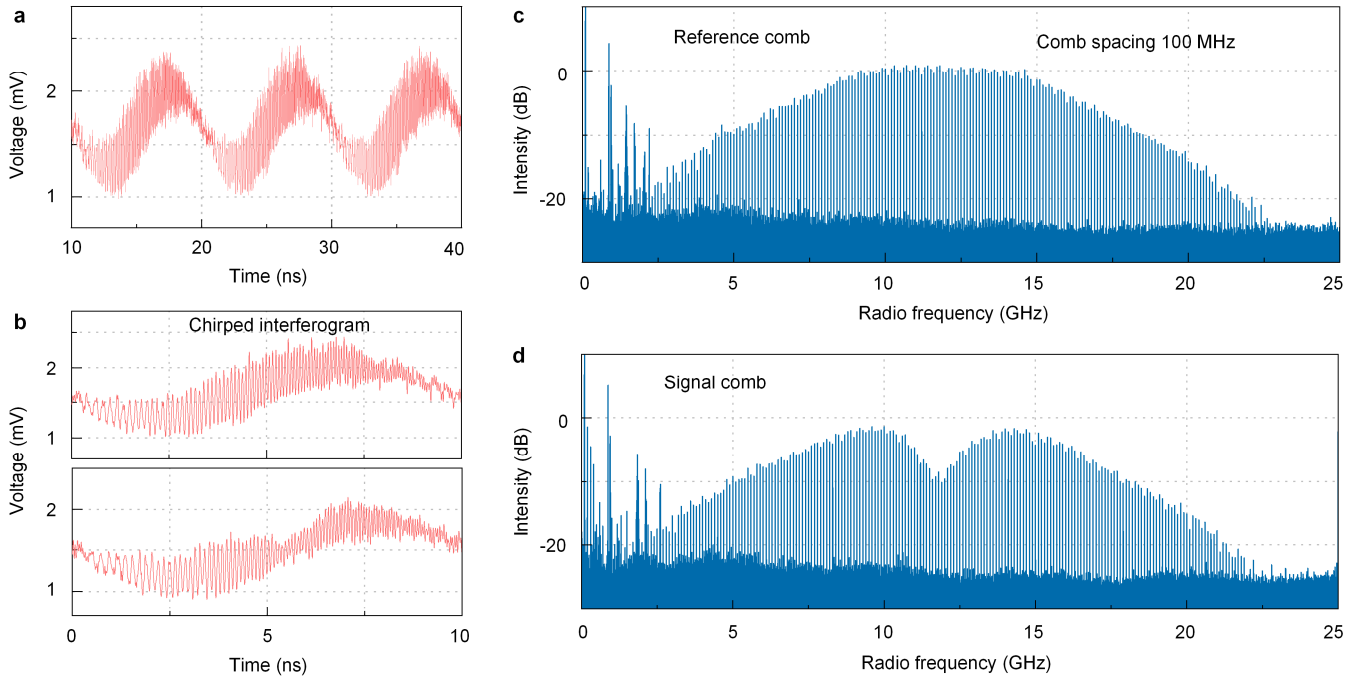


**Fig. 3 | Measured electrical interferograms and transformed RF combs.** **a**, Periodically chirped interferogram with period of 10 ns. **b**, Enlarged interferograms. Upper: without absorption feature. Bottom: with absorption feature of  $H^{13}CN$ . **c** and **d**, RF combs obtained by performing Fourier transform on the temporal interferograms with recording time of 25,000 periods. The comb without gas feature function as a reference.

In experiment, the periodically chirped interferogram is shown in Fig. 3a. The enlarged figures in Fig. 3b show chirped frequency of the interferograms over one period. The upper interferogram in Fig. 3b is formed without gas cell, while the bottom interferogram contains the absorption feature in the  $2\nu_3$  band of  $H^{13}CN$ . The RF combs (Fig. 3c and 3d) are obtained by performing FFT on the time-domain waveforms. In order to get a SNR better than 25 dB in the center lines, the interferograms over 25,000 periods are recorded for FFT. Indeed, the minimum acquisition time can be shortened to 10 ns when a better amplifier is adopted. The reference comb and the signal comb in the RF domain have the same comb spacing, which is equal to the repetition frequency of the laser. Here, the optical spectrum with a span of 112.5 GHz in the OF domain is down-converted to a range of about 20.7 GHz in the RF domain, which means over 200 RF comb teeth is recorded corresponding to 0.9 nm optical spectrum.

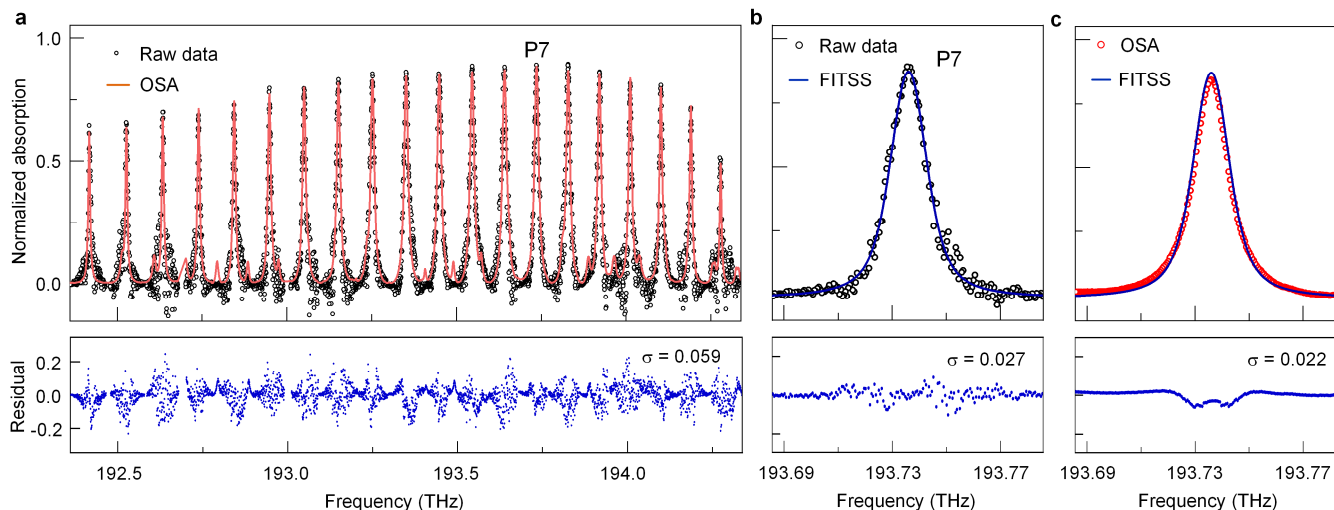


**Fig. 4 | Measured molecular absorption spectra.** **a**, Absorption features in the  $2\nu_3$  band of  $\text{H}^{13}\text{CN}$  are assembled by 20 absorption lines. Overlay of the raw data and the spectrum directly measured by optical spectrum analyzer (OSA) shows line-by-line matching. The standard deviation of the residuals is 0.059. **b**, The result of FITSS is obtained by fitting the raw data with a Voigt function. The resolution of FITSS with laser repetition rate of 100 MHz is 545 MHz. **c**, Comparison of the results from FITSS and OSA.

Finally, after transforming the recorded waveforms, the absorption spectrum is normalized from the peaks of the signal and reference combs. In Fig. 4a, the measured FITSS spectrum (black circles) in the  $2\nu_3$  band of  $\text{H}^{13}\text{CN}$  from 192.36 THz to 194.34 THz is compared with the absorption spectrum measured by an optical spectrum analyzer (OSA). Wide spectrum is acquired by tuning the programmable filter. 20 absorption features are assembled. The line-by-line overlay of measured data from FITSS and OSA shows good uniformity in the overall profiles. Some negative numbers appear in the normalized absorption feature due to the low SNR sample points on the edges of the RF comb. The residual difference between the two absorption spectra is shown as blue dots in Fig. 4a. Then, the raw data of FITSS is fitted with a Voigt function (Fig. 4b). The final FITSS result refers to the fitted curve is compared with the OSA spectrum in Fig. 4c, which confirms the wavelength precision and absorption intensity accuracy of this method. The spectrum resolution is directly determined by the pulse repetition rate of the femtosecond laser source. In this experiment, a pulse repetition frequency of 100 MHz corresponds to an optical frequency resolution of 545 MHz at 1550 nm. Most peaks of the absorption lines in OSA is slightly lower than that in FITSS due to the limited resolution (2.5 GHz) of the OSA.

In conclusion, instead of using two stabilized comb sources, FITSS is demonstrated to down-convert the molecular spectrum from the OF domain to the RF domain by utilizing one femtosecond laser, incorporating time-stretch interferometer with imbalanced dispersion. No phase-lock electronics are required, while passive optical components for the telecommunication industry are predominantly used. Benefiting from time-stretch technique, FITSS is characterized of all-fiber compact structure, high detection sensitivity and resolution, ultrafast data acquisition speed. With further system development, FITSS can be extended to practical applications of non-intrusive and non-repetitive gas monitoring in chemical reaction and remote sensing of gas concentrations in real-time. Simulated Raman amplification<sup>17,21</sup> is superior to compensate the signal power loss in the photonics time-stretch system. Hence, the SNR of FITSS will be further increased. And even single-shot detection can be achieved. For higher spectrum resolution, the density of comb teeth can be increased by decreasing the pulse repetition frequency.

## Reference

1. Coddington, I., Swann, W. C. & Newbury, N. R. Coherent multiheterodyne spectroscopy using stabilized optical frequency combs. *Phys. Rev. Lett.* **100**, 11–14 (2008).
2. Picqué, N. & Hänsch, T. W. Frequency comb spectroscopy. *Nat. Photonics* **13**, 146–157 (2019).
3. Coddington, I., Newbury, N. & Swann, W. Dual-comb spectroscopy. *Optica* **3**, 414–426 (2016).
4. Millot, G., Pitois, S., Yan, M., Hovhannisyan, T., Bendahmane, A., Hänsch, T. W. & Picqué, N. Frequency-agile dual-comb spectroscopy. *Nat. Photonics* **10**, 27–30 (2016).
5. Keilmann, F., Gohle, C. & Holzwarth, R. Time-domain mid-infrared frequency-comb spectrometer. *Opt. Lett.* **29**, 1542 (2004).
6. Ideguchi, T., Poisson, A., Guelachvili, G., Picqué, N. & Hänsch, T. W. Adaptive real-time dual-comb spectroscopy. *Nat. Commun.* **5**, 3375 (2014).
7. Ycas, G., Giorgetta, F. R., Baumann, E., Coddington, I., Herman, D., Diddams, S. A. & Newbury, N. R. High-coherence mid-infrared dual-comb spectroscopy spanning 2.6 to 5.2  $\mu\text{m}$ . *Nat. Photonics* **12**, 202–208 (2018).
8. Lomsadze, B. & Cundiff, S. T. Frequency combs enable rapid and high-resolution multidimensional coherent spectroscopy. *Science* **357**, 1389–1391 (2017).
9. Coburn, S., Alden, C. B., Wright, R., Cossel, K., Baumann, E., Truong, G.-W., Giorgetta, F., Sweeney, C., Newbury, N. R., Prasad, K., Coddington, I. & Rieker, G. B. Regional trace-gas source attribution using a field-deployed dual frequency comb spectrometer. *Optica* **5**, 320–327 (2018).
10. Ycas, G., Giorgetta, F. R., Cossel, K. C., Waxman, E. M., Baumann, E., Newbury, N. R. & Coddington, I. Mid-infrared dual-comb spectroscopy of volatile organic compounds across long open-air paths. *Optica* **6**, 165–168 (2019).
11. Suh, M.-G., Yang, Q.-F., Yang, K. Y., Yi, X. & Vahala, K. J. Microresonator soliton dual-comb spectroscopy. *Science* **354**, 600–603 (2016).
12. Gaeta, A. L., Lipson, M. & Kippenberg, T. J. Photonic-chip-based frequency combs. *Nat. Photonics* **13**, 158–169 (2019).
13. Dutt, A., Joshi, C., Ji, X., Cardenas, J., Okawachi, Y., Luke, K., Gaeta, A. L. & Lipson, M. On-chip dual-comb source for spectroscopy. *Sci. Adv.* **4**, e1701858 (2018).
14. Yu, M., Okawachi, Y., Griffith, A. G., Picqué, N., Lipson, M. & Gaeta, A. L. Silicon-chip-based mid-infrared dual-comb spectroscopy. *Nat. Commun.* **9**, 6–11 (2018).
15. Link, S. M., Maas, D. J. H. C., Waldburger, D. & Keller, U. Dual-comb spectroscopy of water vapor with a free-running semiconductor disk laser. *Science* **356**, 1164–1168 (2017).
16. Ideguchi, T., Nakamura, T., Kobayashi, Y. & Goda, K. Kerr-lens mode-locked bidirectional dual-comb ring laser for broadband dual-comb spectroscopy. *Optica* **3**, 748 (2016).
17. Mahjoubfar, A., Churkin, D. V., Barland, S., Broderick, N., Turitsyn, S. K. & Jalali, B. Time stretch and its applications. *Nat. Photonics* **11**, 341–351 (2017).
18. Solli, D. R., Chou, J. & Jalali, B. Amplified wavelength-time transformation for real-time spectroscopy. *Nat. Photonics* **2**, 48–51 (2008).
19. Chou, J., Solli, D. R. & Jalali, B. Real-time spectroscopy with subgigahertz resolution using amplified dispersive Fourier transformation. *Appl. Phys. Lett.* **92**, 3–6 (2008).
20. Goda, K. & Jalali, B. Dispersive Fourier transformation for fast continuous single-shot measurements. *Nat. Photonics* **7**, 102–112 (2013).

21. Goda, K., Tsia, K. K. & Jalali, B. Serial time-encoded amplified imaging for real-time observation of fast dynamic phenomena. *Nature* **458**, 1145–1149 (2009).
22. Goda, K., Ayazi, A., Gossett, D. R., Sadasivam, J., Lonappan, C. K., Sollier, E., Fard, A. M., Hur, S. C., Adam, J., Murray, C., Wang, C., Brackbill, N., Di Carlo, D. & Jalali, B. High-throughput single-microparticle imaging flow analyzer. *Proc. Natl. Acad. Sci.* **109**, 11630–11635 (2012).
23. Nakagawa, K., Iwasaki, A., Oishi, Y., Horisaki, R., Tsukamoto, A., Nakamura, A., Hiroasawa, K., Liao, H., Ushida, T., Goda, K., Kannari, F. & Sakuma, I. Sequentially timed all-optical mapping photography (STAMP). *Nat. Photonics* **8**, 695–700 (2014).
24. Xia, H. & Zhang, C. Ultrafast ranging lidar based on real-time. *Opt. Lett.* **34**, 2108–2110 (2009).
25. Xia, H. & Zhang, C. Ultrafast and Doppler-free femtosecond optical ranging based on dispersive frequency-modulated interferometry. *Opt. Express* **18**, 4118–4129 (2010).
26. Herink, G., Kurtz, F., Jalali, B., Solli, D. R. & Ropers, C. Real-time spectral interferometry probes the internal dynamics of femtosecond soliton molecules. *Science* **356**, 50–54 (2017).
27. Wang, C., Zeng, F. & Yao, J. All-fiber ultrawideband pulse generation based on spectral shaping and dispersion-induced frequency-to-time conversion. *IEEE Photonics Technol. Lett.* **19**, 137–139 (2007).
28. Chi, H. & Yao, J. All-Fiber Chirped Microwave Pulses Generation Based on Spectral Shaping and Wavelength-to-Time Conversion. *IEEE Trans. Microw. Theory Tech.* **55**, 1958–1963 (2007).
29. Wang, C. & Yao, J. Chirped Microwave Pulse Generation Based on Optical Spectral Shaping and Wavelength-to-Time Mapping Using a Sagnac Loop Mirror Incorporating a Chirped Fiber Bragg Grating. *J. Light. Technol.* **27**, 3336–3341 (2009).
30. Xia, H. & Yao, J. Characterization of subpicosecond pulses based on temporal interferometry with real-time tracking of higher order dispersion and optical time delay. *J. Light. Technol.* **27**, 5029–5037 (2009).

## Acknowledgements

This work was supported by the Anhui Initiative in Quantum Information Technologies.

## Author contributions

H.Y.X. conceived the idea. Z.Z., S.F.Y. and L.J.Z. performed the experiment under the guidance of H.Y.X. and X.K.D. All authors contributed to the discussion of experimental results. Z.Z. wrote the manuscript with contributions from all co-authors. H.Y.X. and X.K.D. supervised the project.

## Additional information

Correspondence and request for materials should be addressed to H.Y.X.

## Competing financial interests

The authors declare no competing financial interests.

## Methods

**Time-to-frequency mapping function.** After passing through a DCF, the femtosecond pulse is dispersed and stretched, and the spectral information is mapping to the time domain by GVD. FITSS is a time-stretch interferometry, where the dispersion

values in the two arms are different. Based on the instantaneous frequency concept in time-stretch<sup>25</sup>, considering dispersion up to the third-order, the instantaneous frequency  $\omega_p$  of the probing pulse can be expressed as

$$\omega_p(t) = t/\beta_2 L_0 - \beta_3 L_0 t^2 / 2(\beta_2 L_0)^3 \quad (1)$$

where  $\omega$  is the angular frequency relative to the center frequency of the pulse,  $t$  is the relative group delay time,  $L_0$  is the length of DCF in the time-stretch module in Fig. 2,  $\beta_2 = 210 \text{ ps}^2 \text{ km}^{-1}$  and  $\beta_3 = -1.289 \text{ ps}^3 \text{ km}^{-1}$  are the second-order and third-order mode-propagation constant, respectively. The units of time and frequency are picosecond and terahertz, respectively. The reference pulse transmits through an optical delayer and an additional DCF, so that the instantaneous frequency  $\omega_r$  of the reference pulse can be expressed as

$$\omega_r(t) = (t - \tau)/\beta_2(L_0 + L_1) - \beta_3(L_0 + L_1)(t - \tau)^2 / 2[\beta_2(L_0 + L_1)]^3 \quad (2)$$

where  $\tau$  and  $L_1$  are the time delay and the length of DCF for imbalanced dispersion in the reference arm of MZI (Fig. 2), respectively. Due to the narrow bandwidth of the programmable filter used in this work, the time-to-frequency mappings process are almost linear. The coefficients of determination  $R^2$  of linear fitting of the equations (1) and (2) are nearly equal to 1, and the sum of squares of residuals are  $1.14 \times 10^{-7}$  and  $5.03 \times 10^{-8}$ , respectively. For simplicity, the following discussion will consider dispersion up to group delay dispersion.

**Heterodyne detection.** As shown in Fig. 2f, the probing and reference pulses are separated from a Gaussian shaped pulse, then the probing pulse is absorbed after passing through the  $\text{H}^{13}\text{CN}$  gas cell, whose absorption function can be seen as a Voigt function. So the spectrum intensity in two arms of MZI can be expressed as  $I_p(\omega) = G_{\text{Gauss}}(\omega)[1 - G_{\text{Voigt}}(\omega)]$  and

$I_r(\omega) = G_{\text{Gauss}}(\omega)$ . The complex spectrum can be expressed as  $a_p(\omega) = [I_p(\omega)]^{0.5} \varphi(j\omega)$  and  $a_r(\omega) = [I_r(\omega)]^{0.5} \varphi(j\omega)$ . The chromatic dispersion up to group delay dispersion performs an optical Fourier transform to the pulse<sup>30</sup>. The reference pulse transmits through an optical delayer and an additional DCF. So considering the dispersion up to group delay dispersion, the complex pulse<sup>30</sup> can be expressed as

$$a_p(t) = h_p \exp(jt^2 / 2\beta_2 L_0) [a_p(\omega)]_{\omega=t/\beta_2 L_0} \quad (3)$$

$$a_r(t) = h_r \exp[j(t - \tau)^2 / 2\beta_2(L_0 + L_1)] [a_r(\omega)]_{\omega=(t-\tau)/\beta_2(L_0+L_1)} \quad (4)$$

where  $h_p = H_0 (j2\pi\beta_2 L_0)^{-0.5} \exp(-j\beta_0 L_0)$  and  $h_r = H_0 [j2\pi\beta_2(L_0 + L_1)]^{-0.5} \exp[-j\beta_0(L_0 + L_1)]$  are the complex amplitude of the two complex pulse.  $H_0$  is a constant of the fiber transmission rate and  $\beta_0$  is the zero-order mode-propagation constant.



For simplicity, the following equations are introduced  $C_p = h_p \exp(jt^2 / 2\beta_2 L_0)$  and  $C_r = h_r \exp[j(t-\tau)^2 / 2\beta_2 (L_0 + L_1)]$ .

Hence equations (3) and (4) can be expressed as

$$a_p(t) = C_p [G_{\text{Gauss}}(t / \beta_2 L_0)]^{0.5} [1 - G_{\text{Voigt}}(t / \beta_2 L_0)]^{0.5} \exp[j\phi(t / \beta_2 L_0)] \quad (5)$$

$$a_r(t) = C_r \{G_{\text{Gauss}}[(t-\tau) / \beta_2 (L_0 + L_1)]\}^{0.5} \exp\{j\phi[(t-\tau) / \beta_2 (L_0 + L_1)]\} \quad (6)$$

The probing and reference pulses are combined by a coupler and fed to a PD. The interference term of the detector response photocurrent can be derived from equations (5) and (6)

$$i(t) = [G_{\text{envelope}}(t)]^{0.5} [1 - G_{\text{Voigt}}(t / \beta_2 L_0)]^{0.5} \cos[\Delta\omega(t)t] \quad (7)$$

where  $G_{\text{envelope}}(t) = |C_p| |C_r| G_{\text{Gauss}}[(t-\tau) / \beta_2 (L_0 + L_1)] G_{\text{Gauss}}(t / \beta_2 L_0)$  is the envelope without absorption feature.

$|C_p| = H_0 (2\pi\beta_2 L_0)^{-0.5}$  and  $|C_r| = H_0 [2\pi\beta_2 (L_0 + L_1)]^{-0.5}$  are constants.  $\Delta\omega(t) = |\omega_p(t) - \omega_r(t)|$  is the beat frequency. Using

equations (1) and (2), the beat frequency can be expressed as  $\Delta\omega(t) = t / \beta_2 L_0 - (t-\tau) / \beta_2 (L_0 + L_1)$ . If there is no imbalanced

dispersion, i.e.,  $L_1 = 0$ , the beat frequency will be a constant  $\Delta\omega = \tau / \beta_2 L_0$ . While the imbalanced dispersion is employed in

FITSS, the beat frequency is chirped over about 20 GHz. By performing FFT to  $i(t)$  in equation (7), the absorption feature is retrieved in the envelope of the wideband RF spectrum.

**Dual-comb spectroscopy.** Dual-comb spectroscopy is a comb-based Fourier transform interferometry without moving parts.

In DCS, two optical frequency combs with slightly different repetition frequency ( $f_{\text{rep}}$  and  $f_{\text{rep}} + \Delta f_{\text{rep}}$ ) are heterodyned,

generating a down-converted RF comb which contains information encoded in the OF combs. In the time domain, the pulses

from one comb ( $f_{\text{rep}}$ ) walk through the pulses of the second comb ( $f_{\text{rep}} + \Delta f_{\text{rep}}$ ) with a time delay that automatically increases

by an amount  $\Delta f_{\text{rep}} / f_{\text{rep}}^2$  from pulse pair to pulse pair<sup>2</sup>. The first comb is optically sampled by the second comb, providing

an interferogram stretched in time by a factor of  $f_{\text{rep}} / \Delta f_{\text{rep}}$ . In the frequency domain, the beat signal of the two combs

produces a comb with comb spacing of  $\Delta f_{\text{rep}}$  in the RF domain that can directly be measured by digital electronics. The

one-to-one mapping between OF comb and RF comb is built.